


|  |   |          |       |                     |         |
|--|---|----------|-------|---------------------|---------|
|  | <p><i>Multilayer Coatings for High-Energy Optics for Astrophysics</i></p> <p><b>Optics 346 manufactured at MSFC and Harvard-CfA: results of tests at PANTER facility and surface characterization</b></p> |          |       |                     |         |
| Code:01/07   | INAF/OAB Technical Report   | Issue: 1 | Class | <b>CONFIDENTIAL</b> | Page: 1 |

*Multilayer Coatings for High-Energy Optics for Astrophysics*

## **X-ray optic 346 manufactured at MSFC and Harvard-CfA: results of tests at PANTER facility and surface characterization**

*Issued by **D. Spiga** (INAF/OAB, Merate, Italy)*

*Data reduction by **D. Spiga** and **R. Canestrari** (INAF/OAB, Merate, Italy)*

*Mirror shells electroformed by MSFC/NASA (Huntsville, AL, USA) under supervision of **B. Ramsey***



*Multilayer coating deposited at the Harvard – Smithsonian Center for Astrophysics (Boston, MA, USA) by **S. Romaine, P. Gorenstein, R. Bruni***

*X-ray measurements performed by PANTER (MPE, Garching, Germany) team - **M. Freyberg, W. Burkert, G. Hartner, B. Budau**.*

*Mirror shell integration by **S. Basso, F. Mazzoleni, R. Valtolina** (INAF/OAB)*

*AFM measurements by **R. Valtolina** (INAF/OAB)*

*Reviewed by **G. Pareschi** (INAF/OAB)*

|   |   |          |       |                     |         |
|---|---|----------|-------|---------------------|---------|
|   | <p align="center"><i>Multilayer Coatings for High-Energy Optics for Astrophysics</i></p> <p align="center"><b>Optics 346 manufactured at MSFC and Harvard-CfA: results of tests at PANTER facility and surface characterization</b></p> |          |       |                     |         |
| Code:01/07  | INAF/OAB Technical Report   | Issue: 1 | Class | <b>CONFIDENTIAL</b> | Page: 2 |

## Contents


|   |           |
|---|-----------|
| <b>1. Introduction.....</b>   | <b>4</b>  |
| <b>2. Results of tests at PANTER and INAF/OAB .....</b>                 | <b>5</b>  |
| 2.1 – Witness mirror sample: X-ray reflectivity tests.....              | 5         |
| 2.2 – PANTER data reduction .....                                       | 7         |
| 2.3 – Mirror shell 346, geometrical properties .....                    | 8         |
| 2.4 – PANTER results: effective areas .....                             | 9         |
| 2.5 – PANTER results: Half Energy Widths.....                           | 11        |
| <b>3 – Metrological tests performed at INAF/OAB.....</b>                | <b>12</b> |
| 3.1- Microroughness and profiles measurements .....                     | 12        |
| 3.2 – Interpretation of mirror shell HEW trend .....                    | 14        |
| 3.2.1- <i>Compton Scattering in the Silicon pn-EPIC detector?</i> ..... | 14        |
| 3.2.2- <i>X-ray scattering from surface microroughness</i> .....        | 16        |
| 3.3 – Conclusions.....  | 18        |

## Applicable Documents

[AD1] D. Spiga et al., *Multilayer-coated mirror shell test at PANTER facility: Preliminary Performances Evaluation and Test Plan Definition*, **INAF/OAB technical report 01/06**

## Reference Documents


- [RD1] S. Romaine et al., *Development of a prototype Nickel Optic for the Constellation-X Hard X-ray telescope: III* - **SPIE Proc.** 5900 p. 225-231
- [RD2] H. Bräuninger et al., *Calibration of hard X-ray (15 – 50 keV) optics at the MPE test facility PANTER* -**SPIE Proc.** 5168, p. 283-293
- [RD3] D. Spiga et al., *Characterization of multilayer stack parameters from X-ray reflectivity data using the PPM program: measurements and comparison with TEM results* - **SPIE Proc.** 6266, p. 626616
- [RD4] D. Spiga et al., *Mirror shell 338 (Jet-X mandrel n. 1 sized - shell): achieved tests at PANTER facility and INAF/OAB (July 2005)*, **INAF/OAB Internal Report 02/06**

|  |   |          |       |                     |         |
|--|---|----------|-------|---------------------|---------|
|  | <p><i>Multilayer Coatings for High-Energy Optics for Astrophysics</i></p> <p><b>Optics 346 manufactured at MSFC and Harvard-CfA: results of tests at PANTER facility and surface characterization</b></p> |          |       |                     |         |
| Code:01/07   | INAF/OAB Technical Report   | Issue: 1 | Class | <b>CONFIDENTIAL</b> | Page: 3 |

[RD5] D. Spiga, *Analytical evaluation of the X-ray scattering contribution to imaging degradation in grazing-incidence X-ray telescopes*, *Astronomy and Astrophysics*, Vol. 468, issue 2, pp. 775-784

## Acronyms

CCD Charge-Coupling Device  
HEW Half-Energy Width  
INAF Istituto Nazionale di AstroFisica / *Italian Institute for Astrophysics*  
MPE Max-Planck Institut für Extraterrestrische Physik /*Max Planck Institute for Extraterrestrial Physics*  
MSFC Marshall Space Flight Center  
OAB Osservatorio Astronomico di Brera / *Brera Astronomical Observatory*  
PSD Power Spectral Density  
PSPC Position-Sensitive Proportional Counter  
ROI Region Of Interest  
UV UltraViolet

|  |   |          |       |                     |         |
|--|---|----------|-------|---------------------|---------|
|  | <p align="center"><i>Multilayer Coatings for High-Energy Optics for Astrophysics</i></p> <p align="center"><b>Optics 346 manufactured at MSFC and Harvard-CfA: results of tests at PANTER facility and surface characterization</b></p> |          |       |                     |         |
| Code:01/07   | INAF/OAB Technical Report   | Issue: 1 | Class | <b>CONFIDENTIAL</b> | Page: 4 |

## 1. Introduction

Aim of this document is to report on the soft and hard X-rays characterization of a multilayer-coated optic (with 10 m focal length) after full-illumination measurements at the PANTER facility in full-illumination setup (MPE, Garching, Germany), followed by a set of metrological and surface microroughness tests dealt at INAF/OAB.

The optic prototype (named **346** in the following) was a single Wolter I mirror shell with a diameter of 230 mm, an on-axis incidence angle of 0.165 deg. The mirror shell substrate - with 100  $\mu\text{m}$  thick mirror walls - has been manufactured at the MSFC by Ni-Co electroforming of preformed mandrels. The mirror shell was coated with a W/Si graded multilayer by magnetron sputtering using a facility specifically conceived to coat mirror shells [RD1], in order to enhance the reflectivity in hard X-rays. During the mirror shell coating run a small (2 in. diam.) superpolished fused silica sample was also coated as “witness” of process. The very high optical finishing level of this substrate ( $\sigma < 2 \text{ \AA}$ ) has a negligible contribution in the final multilayer roughness, therefore the final microroughness of this witness sample returns, in practice, the intrinsic microroughness developed in the deposition process. Thus, its contribution to mirror shell microroughness can be disentangled from the initial substrate quality. Finally, the shell was integrated at INAF/OAB in a stainless steel case in order to provide it with the correct shape and mechanical rigidity during the optic handling at PANTER. The integration was performed in the UV optical bench available at INAF/OAB.

|  |   |          |       |                     |         |
|--|---|----------|-------|---------------------|---------|
|  | <p align="center"><i>Multilayer Coatings for High-Energy Optics for Astrophysics</i></p> <p align="center"><b>Optics 346 manufactured at MSFC and Harvard-CfA: results of tests at PANTER facility and surface characterization</b></p> |          |       |                     |         |
| Code:01/07   | INAF/OAB Technical Report   | Issue: 1 | Class | <b>CONFIDENTIAL</b> | Page: 5 |

## 2. Results of tests at PANTER and INAF/OAB

### 2.1 – Witness mirror sample: X-ray reflectivity tests

The W/Si multilayer coating was structured as a double stack. The outer stack is formed by 20, thicker bilayers, and the inner stack has 75 thinner bilayers, devoted to the reflection of the hardest part of the X-ray spectrum. The d-spacing trend in the stack follows the well-known power-law of supermirrors:

$$d(k) = \frac{a}{(k+b)^c}$$

where  $k = 1, 2, \dots$  and  $a, b, c$  are parameters that can be optimized in order to achieve the maximum reflectivity in the band of interest. The witness mirror sample was used to investigate the actual structure of the multilayer stack by means of X-ray reflectivity (XRR) analysis. The XRR measurement was performed at the fixed energy of 8.05 keV (the Cu  $K\alpha_1$  X-ray line) and the reflectance as a function of incidence angle is shown in Fig. 1 (red line). The natural densities of W and Si were assumed.

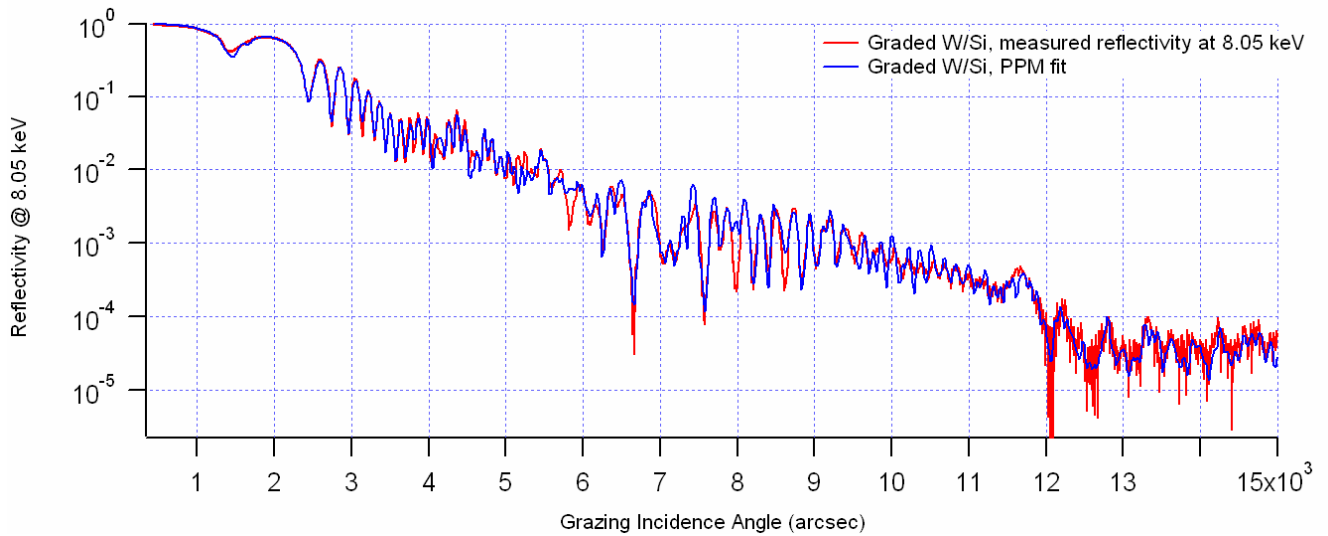



Fig. 1: reflectance plot at 8.05 keV of multilayer witness mirror. Logarithmic plot. The agreement of data (red line) with model (blue line) is very satisfactory.

The extraction of stack parameters was done by means of the PPM program [RD3], which is able to find the stack structure which returns the best fit of reflectance scan. The multilayer structure model was assumed to follow independent power laws for W and Si in each stack. The thickness of each layer can, in addition, oscillate independently around the values calculated from the power-law trend to include short-term thickness instability. Moreover, in order to reach the best fit of the reflectivity, the multilayer roughness has been assumed to vary linearly with the bilayer index throughout each stack. The final reflectivity model found by PPM (blue line) is in excellent agreement with the experimental reflectance (Fig. 1). We show in Fig. 2 the derived thickness trend for both W

|  |   |          |       |                     |         |  |
|--|---|----------|-------|---------------------|---------|--|
|  | <p align="center"><i>Multilayer Coatings for High-Energy Optics for Astrophysics</i></p> <p align="center"><b>Optics 346 manufactured at MSFC and Harvard-CfA: results of tests at PANTER facility and surface characterization</b></p> |          |       |                     |         |  |
| Code:01/07   | INAF/OAB Technical Report   | Issue: 1 | Class | <b>CONFIDENTIAL</b> | Page: 6 |  |

and Si, and the best-fitting power-laws in the two stacks: the power-law parameters are reported in Tab.1. In addition, the automatic fitting procedure finds an evident increase of  $\sigma$ , from 3.0 Å close to the fused silica substrate to 4.1 Å at the end of the first (deepest) stack. The roughness drifts from 4.2 to 4.3 Å in the outer stack: the smaller increase in the outer stack can be partly due to the smaller total thickness (0.128  $\mu\text{m}$  vs. 0.237  $\mu\text{m}$  of the inner stack, see Tab. 1), but it is not sufficient to explain it completely. The reduction of roughening rate can also be caused by a saturation of the roughening process.

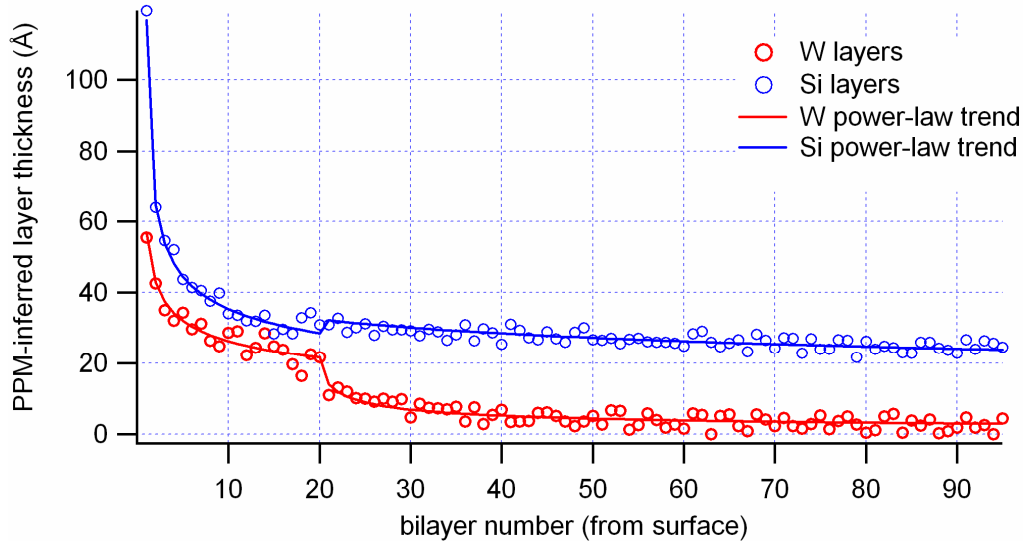



Fig. 2: thickness trend inferred the PPM fit (circles): the two power-law trends (for W and Si) are also superposed to data (solid lines). The break is clearly visible at the 20<sup>th</sup> bilayer. The actual thickness values oscillate around the power-law trend up to a maximum of  $\pm 3$  Å.

Tab. 1: characteristic parameters of the two power law of the adopted graded multilayer. The random term with a maximum amplitude of 3 Å (see Fig. 3) is not considered.

|                                    | a (Å) | b     | c    | appr. $d_{\text{max}} - d_{\text{min}}$ (Å) | total thicken. (Å) |
|------------------------------------|-------|-------|------|---|--------------------|
| 1 <sup>st</sup> stack Si (20 bil.) | 67.30 | -0.87 | 0.29 | 122– 29                                     | 745                |
| 1 <sup>st</sup> stack W (20 bil.)  | 48.37 | -0.46 | 0.27 | 57 - 22                                     | 535                |
| 2 <sup>nd</sup> stack Si (75 bil.) | 68.68 | 28.10 | 0.23 | 32- 24                                      | 1983               |
| 2 <sup>nd</sup> stack W (75 bil.)  | 19.71 | 0.89  | 0.43 | 15 – 3                                      | 390                |

A further test was performed using the X-ray continuum (7 – 50 keV) emitted by a W- anode tube with bias at 50 kV, impinging on the sample at 0.231 deg: this angle is close to the incidence angle on the parabola of the optic at the PANTER (0.218 deg). However, the size of the sample did not enable the collection of all the incident beam at such small angles. The incident and the reflected beam were analyzed by means of a Silicon solid-state detector. The resulting reflectivity is plotted in Fig. 3 with the reflectivity derived from the stack model with parameters listed in Tab. 1, and a constant roughness rms of 4.5 Å. The agreement is quite good.

|  |   |          |       |                     |         |
|--|---|----------|-------|---------------------|---------|
|  | <p style="text-align: center;"><i>Multilayer Coatings for High-Energy Optics for Astrophysics</i></p> <p style="text-align: center;"><b>Optics 346 manufactured at MSFC and Harvard-CfA: results of tests at PANTER facility and surface characterization</b></p> |          |       |                     |         |
| Code:01/07   | INAF/OAB Technical Report   | Issue: 1 | Class | <b>CONFIDENTIAL</b> | Page: 7 |

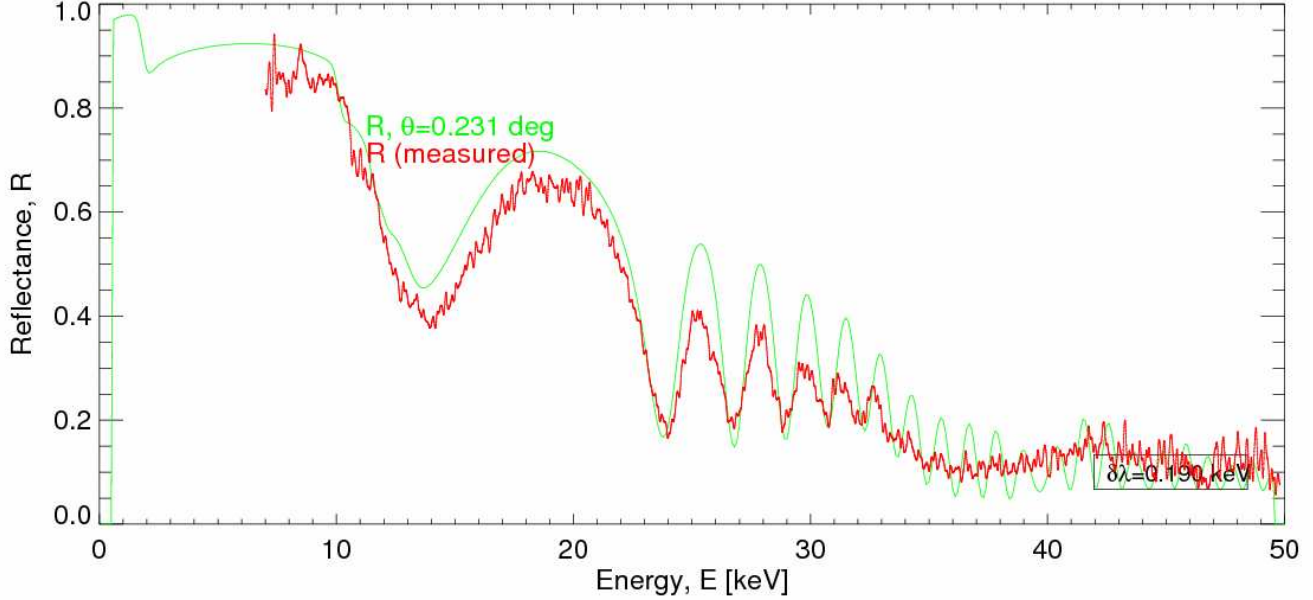


Fig. 3: Reflectivity plot in energy-dispersive setup of the witness mirror, at an incidence angle of 0.231 deg, taken at INAF/OAB using a W- anode X-ray tube (50 kV bias) and a Si detector with a multi-channel analyzer. The experimental curve (red line) is satisfactory agreement with the model with the parameters listed in Tab.1.

## 2.2 – PANTER data reduction

The effective area measurement from detector data is computed from the reflected count rate  $C_M$  in the PSPC or pn-EPIC detector field, measured in a circular region surrounding the focal spot. From the incident X-ray flux  $C_d$  measured from a count rate measurement of the direct beam emerging from a hole of known area  $A_d$ , the mirror effective area at the considered photon energy is simply calculated as


$$A_E(E) = \frac{C_M(E)}{C_d(E)} A_d$$

In energy-dispersive setup the same formula can be applied for each energy channel. The reflectivities of parabola  $R_H^{\alpha+\theta}(E)$  and hyperbola  $R_P^{\alpha-\theta}(E)$  are in general different, because of the finite source distance that causes a beam divergence. The product of the two reflectivities (mirror efficiency) follows from the effective area,

$$R_P^{\alpha+\vartheta}(E) R_H^{\alpha-\vartheta}(E) = \frac{A_E(E)}{A_G^{hp}}$$

where  $A_G^{hp}(E)$  is the mirror shell geometrical cross section for double reflection, accounting for all vignetting due to the finite distance and the spiders (see [AD1] for details). By assuming the mirror



|  |   |          |       |                     |         |
|--|---|----------|-------|---------------------|---------|
|  | <p align="center"><i>Multilayer Coatings for High-Energy Optics for Astrophysics</i></p> <p align="center"><b>Optics 346 manufactured at MSFC and Harvard-CfA: results of tests at PANTER facility and surface characterization</b></p> |          |       |                     |         |
| Code:01/07   | INAF/OAB Technical Report   | Issue: 1 | Class | <b>CONFIDENTIAL</b> | Page: 8 |

shell coating to have the same structure as that of witness mirror (derived in the previous section from XRR scans), but a larger roughness since the two substrates have different starting smoothness levels, the theoretical mirror efficiency can be calculated as a function of the energy and compared with the experimental one. This provides us with important constraints for multilayer roughness. The measurements have been carried out in monochromatic setup using the PSPC detector and the X-ray fluorescence lines listed in Tab. 2, and in energy-dispersive setup (see also [AD1, RD2]) using the pn-EPIC detector.

*Tab.2: X-ray lines used for measurement in monochromatic setup with the PSPC detector*

| <b>Emission line</b> | <b>Energy</b> |
|----------------------|---------------|
| C-K $\alpha$         | 0.27 keV      |
| Cu-L $\alpha$        | 0.93 keV      |
| Al-K $\alpha$        | 1.49 keV      |
| Ag-L $\alpha$        | 2.98 keV      |
| Ti-K $\alpha$        | 4.51 keV      |
| Cr-K $\alpha$        | 5.41 keV      |
| Fe-K $\alpha$        | 6.40 keV      |
| Cu-K $\alpha$        | 8.05 keV      |


## 2.3 – Mirror shell 346, geometrical properties

The mirror shell 346 has a Wolter I profile, with a 10 m nominal focal length and an incidence angle of 0.164 deg for a on-axis source. The geometrical properties and the geometrical cross sections of the integrated mirror shell are listed in Tab.3. We accounted for the finite distance effects as well (see [AD1] for details).

*Tab.3:geometrical properties of the mirror shell 346.*

| <b>Parameter</b>                        | <b>symbol</b>  | <b>value</b>        |
|---|----------------|---------------------|
| maximum mirror diameter (parabola)      | $2R_{max}$     | 231 mm              |
| minimum mirror diameter (hyperbola)     | $2R_{min}$     | 226 mm              |
| mirror length (parabola + hyperbola)    | $2L$           | 427 mm              |
| on-axis incidence angle                 | $\alpha$       | 0.164 deg           |
| focal length (for a source at infinity) | $f$            | 10 m                |
| mirror walls thickness                  | $\tau$         | 100 $\mu$ m         |
| Geometric cross-section from infinity   | $A$            | 4.4 cm <sup>2</sup> |
| Distance source-mirror                  | $X_s$          | $\sim 122$ m        |
| Beam divergence                         | $\theta$       | 0.054 deg           |
| Actual incidence angle on the parabola  | $\alpha_{par}$ | 0.218 deg           |



|  |   |          |       |                     |         |
|--|---|----------|-------|---------------------|---------|
|  | <p style="text-align: center;"><i>Multilayer Coatings for High-Energy Optics for Astrophysics</i></p> <p style="text-align: center;"><b>Optics 346 manufactured at MSFC and Harvard-CfA: results of tests at PANTER facility and surface characterization</b></p> |          |       |                     |         |
| Code:01/07   | INAF/OAB Technical Report   | Issue: 1 | Class | <b>CONFIDENTIAL</b> | Page: 9 |

|   |                       |                     |
|---|-----------------------|---------------------|
| Actual incidence angle on the hyperbola (for <i>double reflection</i> )       | $\alpha_{\text{hyp}}$ | 0.110 deg           |
| Actual image-mirror distance  | $X_i$                 | 10.9 m              |
| Lost area fraction of parabola for double reflection                          | $Q$                   | 49%                 |
| Obscured area fraction by spider  | $V$                   | 10%                 |
| Radius of the parabola single-reflection corona                               | $r_p$                 | 41.9 mm             |
| Radius of the hyperbola single-reflection corona                              | $r_h$                 | 82.8 mm             |
| Geometric cross-section for singly-reflected parabola rays, spider vignettted | $A_g^{\text{par}}$    | 2.6 cm <sup>2</sup> |
| <i>Geometric cross-section for double reflection, spider vignettted</i>       | $A_g^{\text{hp}}$     | 2.7 cm <sup>2</sup> |

## 2.4 – PANTER results: effective areas

Some images of the focal spot of the mirror shell 346 are presented in Fig. 4: we also show in Fig. 5 the measured effective areas for double reflection as measured at PANTER. The data reduction was performed as in Sect. 2.2, using the numerical values of Tab.2. The experimental plot collects the results of PSPC at low energy and those of pn-EPIC at high energies (black circles) for exposures at 30 and 50 kV anode bias. Both effective areas were obtained by integrating the focal spot in a circular ROI of 13.4 mm radius (250 arcsec) around the focus: the size of the ROI is essentially limited by the pn-EPIC edges and by the single-reflection corona, that should be excluded from computation. The circular slits used to exclude the direct beam are wide enough (2.5 mm) to avoid the vignetting of the reflected/scattered beam (as seen from the optic intersection plane they cover a 2400 arcsec angle, much wider than the ROI diameter).

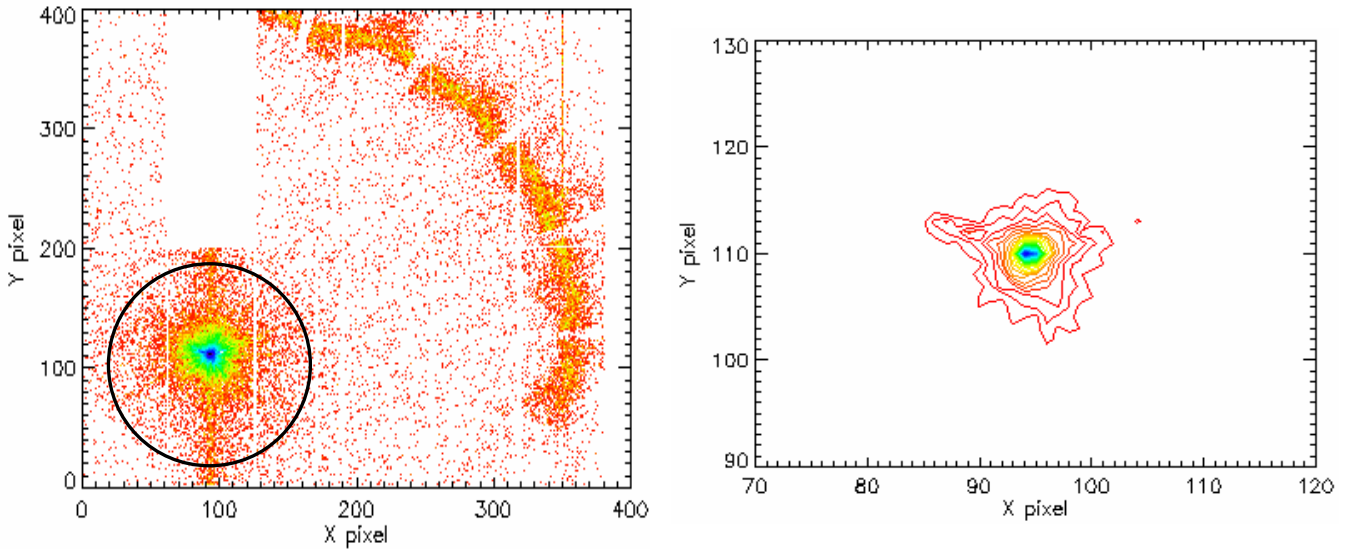



Fig. 4: (left) the focal spot of shell 346 seen by the pn-EPIC in energy dispersive setup up to 50 keV, after 5514 s of exposure time: logarithmic color scale. The edge of adopted ROI is delimited - (right) closer view, contour plot.

|  |   |          |       |                     |          |
|--|---|----------|-------|---------------------|----------|
|  | <p align="center"><i>Multilayer Coatings for High-Energy Optics for Astrophysics</i></p> <p align="center"><b>Optics 346 manufactured at MSFC and Harvard-CfA: results of tests at PANTER facility and surface characterization</b></p> |          |       |                     |          |
| Code:01/07   | INAF/OAB Technical Report   | Issue: 1 | Class | <b>CONFIDENTIAL</b> | Page: 10 |

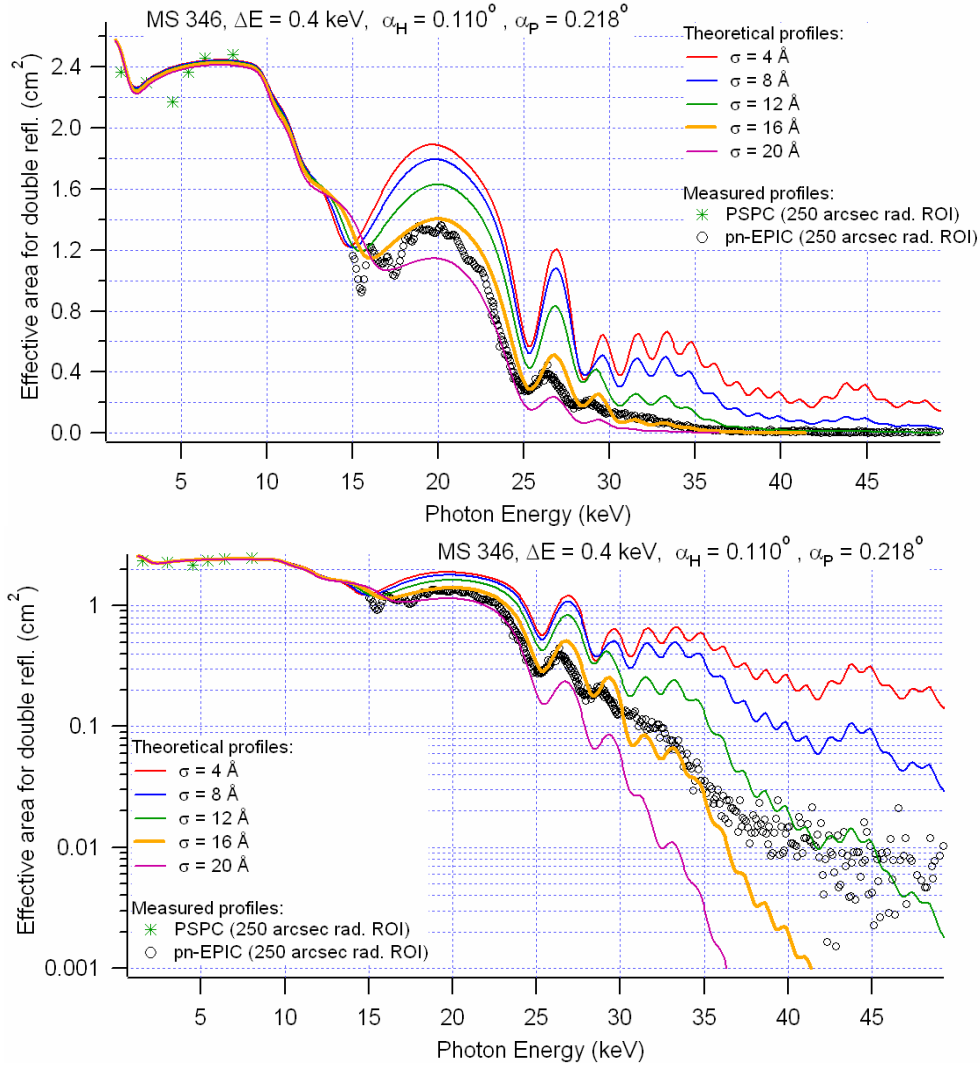



Fig. 5: Measured effective areas of the optic 346 (black circles). Reflectance models for various rms values are also overplotted (solid lines). Linear plot (top) and log plot (bottom)

The reflectivity model, derived from the witness mirror reflectivity scan analysis (sect 2.1) is also overplotted to data (solid lines) for several rms roughness values. The best fitting curve between 15 and 37 keV is obtained setting  $\sigma = 16 \text{ \AA}$  and beyond 37 keV with  $\sigma = 12 \text{ \AA}$  (see also the logarithmic curves). The much larger roughness value than the witness mirror can be ascribed to the much worse smoothness level of substrate with respect to the fused silica substrate of witness. The reflectivity reduction is caused by X-ray scattering, that scatters a relevant amount of radiation out of the ROI, as visible in Fig. 4 (left). In Fig. 4 (right) a close view on the focal spot shows a “baffle” visible in the contour plot. This anisotropy of the PSF can be caused by a mirror deformation in correspondence to a spider bonding.

|  |   |          |       |                     |          |
|--|---|----------|-------|---------------------|----------|
|  | <p style="text-align: center;"><i>Multilayer Coatings for High-Energy Optics for Astrophysics</i></p> <p style="text-align: center;"><b>Optics 346 manufactured at MSFC and Harvard-CfA: results of tests at PANTER facility and surface characterization</b></p> |          |       |                     |          |
| Code:01/07   | INAF/OAB Technical Report   | Issue: 1 | Class | <b>CONFIDENTIAL</b> | Page: 11 |

It is worth noting that the roughness values inferred from the fit are referred to the specific ROI adopted for the integration and should not be assumed as absolute values. From Fig. 5 it can be easily seen that the model with  $\sigma = 16 \text{ \AA}$  overestimates the experiment below 30 keV, whereas the contrary occurs beyond this energy. Summarizing, the best matching of model with  $\sigma \sim 16 \text{ \AA}$  to data is reached around 30 keV including all X-rays scattered within 250 arcsec around the focus, i.e. excluding X-rays scattered by spatial wavelengths smaller than  $13.5 \text{ \mu m}$  for the hyperbola and  $7.7$  on the parabola (we neglect multiple scattering effects).

Using the same argument, the best matching of model with  $\sigma \sim 12 \text{ \AA}$  around 43 keV suggests that this  $\sigma$  value should be obtained by excluding all the X-rays scattered by spatial periods smaller than  $10.7 \text{ \mu m}$  for the hyperbola and  $5.4$  on the parabola.

These results can be compared with the surface PSD calculated from topography (see Sect. 3.1).

## 2.5 – PANTER results: Half Energy Widths

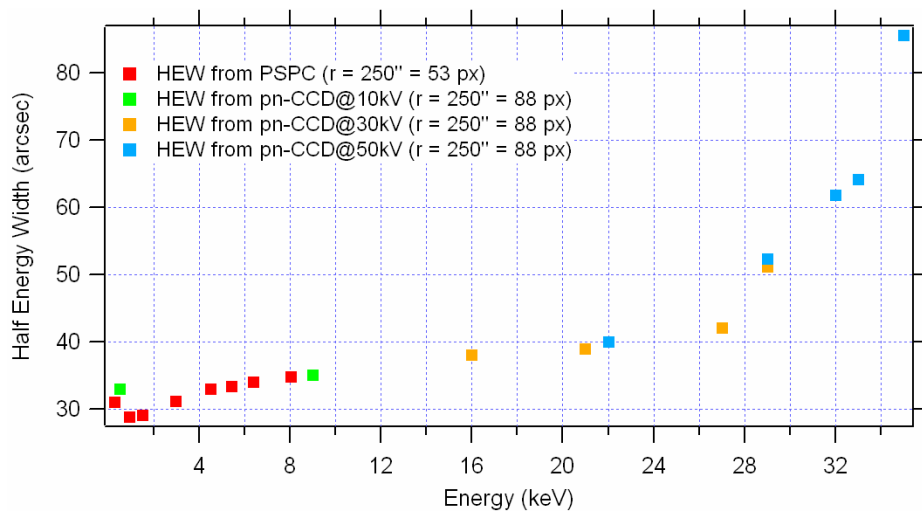



Fig.6: the measured trend of HEW of the shell 346 at the PANTER facility. Collected data of PSPC and pn-EPIC. The HEW are referred to the same ROI radius used for the measurement of effective areas. All HEW values have 2 – 2.3 arcsec uncertainty but at 37 keV (6 arcsec).

The optic HEW as a function of the photon energy has been measured from the PSPC images in monochromatic setup and from pn-EPIC data by filtering events in narrow energy bands ( $\Delta E \sim 2 \text{ keV}$ ). The filtered events are sufficient to return affordable statistics in tracing the PSF and the Encircled Energy which the HEW is computed from. The results are plotted in Fig. 6.

An increase of HEW with photon energy is usually expected as a consequence of the X-ray scattering dependence on the energy: in this case, however, the *HEW trend almost saturates after 15 keV and then rises suddenly after 27 keV*. Moreover, at very low energy an oscillation of the HEW is also visible. The anomalous behaviour around 1 keV can be caused by the scattering from the spider surfaces, that are not optically polished. The steep rise of HEW after 27 keV can be, instead, justified on the basis of the reflecting surface roughness Power Spectral Density (see Sect. 3.2.2).

|  |   |          |       |                     |          |
|--|---|----------|-------|---------------------|----------|
|  | <p align="center"><i>Multilayer Coatings for High-Energy Optics for Astrophysics</i></p> <p align="center"><b>Optics 346 manufactured at MSFC and Harvard-CfA: results of tests at PANTER facility and surface characterization</b></p> |          |       |                     |          |
| Code:01/07   | INAF/OAB Technical Report   | Issue: 1 | Class | <b>CONFIDENTIAL</b> | Page: 12 |

### 3 – Metrological tests performed at INAF/OAB

#### 3.1- Microroughness and profiles measurements

Several surface roughness measurements were taken at INAF/OAB in order to explain the scattering observed at PANTER. A first surface inspection was accomplished using the phase-contrast Nomarski microscope (see Fig. 7). Evident surface defects (mainly randomly-oriented scratches or perpendicular to the optic axis) are visible. In some scans also clear ridges (delaminations?) appear, mainly oriented in the optical axis direction.

Quantitative information on the surface finishing level has been measured with the Digital AFM at INAF/OAB (see Fig. 8). The 100  $\mu\text{m}$  scan ( $\sigma \approx 10 \text{ \AA}$ ) exhibits the topography already observed with the Nomarski microscope (scratches), the 10  $\mu\text{m}$  scan ( $\sigma \approx 9 \text{ \AA}$ ) also shows a grained surface texture. The grains are clearly seen in the 1  $\mu\text{m}$  scan ( $\sigma \approx 6 \text{ \AA}$ ). Although the multilayer growth could contribute to the formation of grains, the inspection of the witness samples deposited for deposition runs (see e.g. [RD4]) for multilayers with similar thickness showed that the intrinsic microroughness rms of the multilayer should not be larger than 2.0-2.5  $\text{\AA}$  for the 1 and 10  $\mu\text{m}$  scan respectively, whereas the rms values for the actual sample are 9 and 6  $\text{\AA}$ . Therefore, most of the observed roughness in the AFM scans is likely to be ascribed to the initial substrate defects.

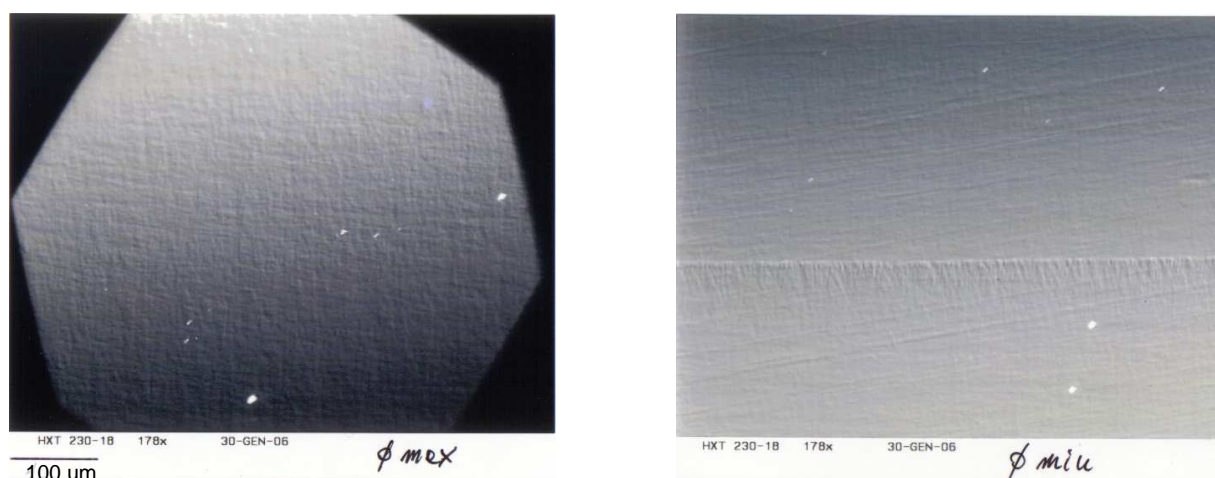



Fig. 7: Nomarski microscope images of the mirror shell samples surface (178x magnification)

The roughness at larger wavelengths has been measured by means of the optical profilometer WYKO. Linear profiles were taken along the optical axis (in the azimuthal direction the measurement was not possible due to the concavity of the specimen) at both 2.5x (2 mm long scans) and 20x (0.66 mm long scans) magnification. This choice allows us covering a wide frequency range that partially overlaps the frequency domain of sensitivity of the AFM.

Also several profiles (20 cm long scans) with the Long Trace Profilometer were taken at INAF/OAB in the axis direction, on both parabola and hyperbola. The results of the measurements are plotted in Fig. 9 in terms of the PSD (Power Spectral Density): all the instruments are in good



|  |   |          |       |                     |          |  |
|--|---|----------|-------|---------------------|----------|--|
|  | <p align="center"><i>Multilayer Coatings for High-Energy Optics for Astrophysics</i></p> <p align="center"><b>Optics 346 manufactured at MSFC and Harvard-CfA: results of tests at PANTER facility and surface characterization</b></p> |          |       |                     |          |  |
| Code:01/07   | INAF/OAB Technical Report   | Issue: 1 | Class | <b>CONFIDENTIAL</b> | Page: 13 |  |

agreement since they overlap in common spectral regions. The most noticeable feature of the PSD of the surface is the double slope change (an “ankle” at  $300\text{ }\mu\text{m}$  and a “knee” at  $0.1\text{ }\mu\text{m}$ ). The PSD at very low frequencies exhibits approximately a power-law trend with a very steep spectral index ( $\sim 2.5$ ): at  $300\text{ }\mu\text{m}$  a spectral break reduces the slope to  $\sim 1$ , followed by a cut-off around  $0.1\text{ }\mu\text{m}$ . The resulting big bump covers the spectral range where the most prominent surface relief features can be observed (see Figs. 7, 8).

The exposed topographical characterization is also consistent with the measured effective area values (see Sect. 2.4): the best-fitting value for the roughness inferred from the fit was  $16\text{ }\text{\AA}$  for the adopted ROI with a  $250\text{ arcsec}$  radius: this integration limit corresponded to a limiting wavelength of  $13.5\text{ }\mu\text{m}$  on the hyperbola and  $7.7\text{ }\mu\text{m}$  on the parabola ( $11\text{ }\mu\text{m}$  on average). If the analysis is correct, the integration of the PSD from  $11\text{ }\mu\text{m}$  to infinity should return a  $\sigma$  value close to  $16\text{ }\text{\AA}$ . The same argument shows that the  $12\text{ }\text{\AA}$  value should be referred to interval of wavelengths smaller than  $7.5\text{ }\mu\text{m}$ .

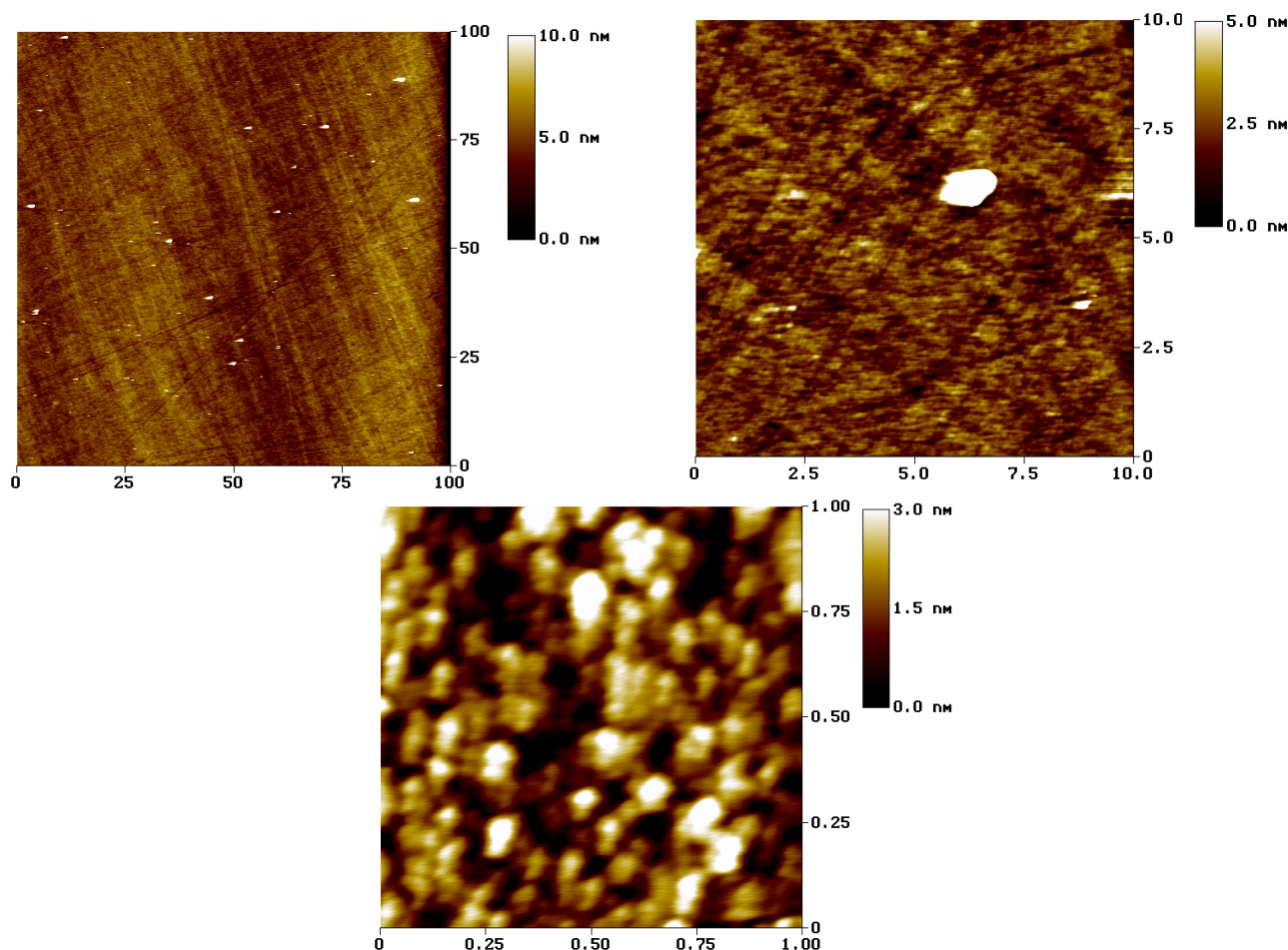



Fig. 8: Some AFM scans of the optic surface samples. 100, 10, 1  $\mu\text{m}$  wide scans. The respective rms values are 12, 13, 8  $\text{\AA}$ .

|  |   |          |       |                     |          |
|--|---|----------|-------|---------------------|----------|
|  | <p align="center"><i>Multilayer Coatings for High-Energy Optics for Astrophysics</i></p> <p align="center"><b>Optics 346 manufactured at MSFC and Harvard-CfA: results of tests at PANTER facility and surface characterization</b></p> |          |       |                     |          |
| Code:01/07   | INAF/OAB Technical Report   | Issue: 1 | Class | <b>CONFIDENTIAL</b> | Page: 14 |

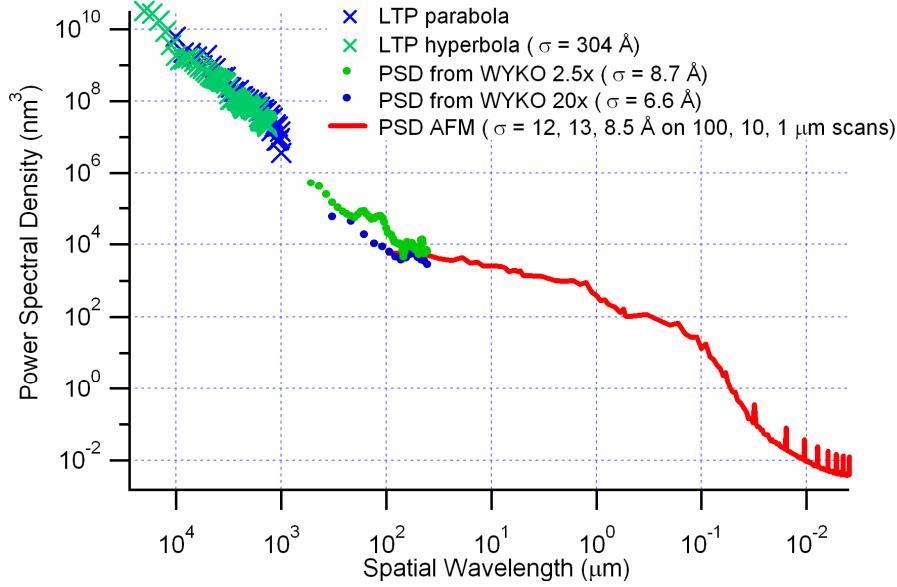


Fig. 9: the surface PSD measured by all the topographic instruments at INAF/OAB. Notice the slope change after 300  $\mu\text{m}$ .

We checked this result by computing the  $\sigma$  parameter from the measured PSD in the mentioned wavelength intervals:

- at spatial wavelengths smaller than 11  $\mu\text{m}$  the integration returns **13 Å (16 expected from the PANTER reflectivity)**
- at spatial wavelengths smaller than 7.5  $\mu\text{m}$  the integration returns **12.5 Å (12 expected from the PANTER reflectivity)**


The residual discrepancy can be ascribed to the approximate procedure in use (i.e. the average of the spatial wavelengths for the two reflections). The PANTER effective area measurement is in good agreement with surface topography results.

### 3.2 – Interpretation of mirror shell HEW trend

#### 3.2.1- Compton Scattering in the Silicon pn-EPIC detector?

In order to interpret the sudden rise of HEW after 27 keV we firstly considered the possibility of Compton Effect in the pn –EPIC Silicon detector, as a result of photon scattering in the plane of the detector: with respect to the photoelectric effect, this effect is usually negligible in soft X-rays and for large-Z elements. The fraction of scattered photons (in any direction) in the pn-EPIC detector is

$$I_{sc} = \tau \rho \frac{f_1}{A} N_A \sigma_c$$

|  |   |          |       |                     |          |
|--|---|----------|-------|---------------------|----------|
|  | <p style="text-align: center;"><i>Multilayer Coatings for High-Energy Optics for Astrophysics</i></p> <p style="text-align: center;"><b>Optics 346 manufactured at MSFC and Harvard-CfA: results of tests at PANTER facility and surface characterization</b></p> |          |       |                     |          |
| Code:01/07   | INAF/OAB Technical Report   | Issue: 1 | Class | <b>CONFIDENTIAL</b> | Page: 15 |

where  $\tau = 300 \mu\text{m}$  is the thickness and  $r = 1.5 \text{ cm}$  the size of the ROI of the Si detector,  $\rho = 2.3 \text{ g/cm}^3$  the density of Silicon,  $f_1$  is the effective atomic number,  $A$  is the Si atomic weight,  $N_A$  is the Avogadro number, and  $\sigma_c$  the Compton cross-section of the electron. As  $h\nu \ll m_e c^2 = 511 \text{ keV}$ , we can approximate it with the Thomson cross-section  $8\pi r_e^2/3$ , with  $r_e = 2.8 \times 10^{-13} \text{ cm}$  is the classical electron radius. From the tabulated value of  $\delta$  at 30 keV (the deviation from 1 of the real part of the refractive index), it is easy to derive the factor  $\rho f_1/A$  appearing in the previous equation, and from this factor, the fraction of scattered photons at 30 keV: 1.4%. It is small, but non negligible with respect to the photoelectric efficiency around 30 keV:  $1 - \exp(-4\pi\beta\tau/\lambda) = 8.2\%$  assuming for  $\beta = 9.1 \times 10^{-10}$ . However, not all scattered photons are also detected: this is clearly illustrated in Fig. 10, where the different cases of scattering at 10 and 30 keV are compared. The fraction of scattered photons in any direction and afterwards detected in the pn-EPIC has a more complicated expression (neglecting multiple Compton scattering events):

$$I_{sc} = \tau \rho \frac{f_1}{A} N_A \int_{-\pi/2}^{+\pi/2} \frac{d\sigma_c}{d\vartheta} \left[ 1 - \exp\left(-\frac{4\pi\beta}{\lambda} z(\vartheta)\right) \right] \cos \vartheta d\vartheta$$



where  $z(\theta)$  is the crossed Si thickness for scattering in the direction  $\theta$  (up to a maximum distance of 1.3 cm – the radius of the adopted ROI). The differential cross-section for non-polarized radiation has the expression  $\pi r_e^2 (1 + \sin^2\theta)$ . Moreover, we can easily compute the average range of scattered photons in the Si detector and, consequently, the HEW due to the Compton effect.

The numerical integration results are listed in Tab.4: the detection of scattered photons is strongly limited by the small thickness of the detector and by the steep decrease of detector sensitivity after 15 keV, and can alter the EA for about 1%. The resulting degradation in imaging quality caused by photon scattering in the pn-EPIC detector increases with the energy of incident photons and reaches 5 arcsec HEW at 50 keV, the maximum investigated photon energy. If we compare this value with the measured 80 arcsec HEW at 37 keV, we conclude that, even though a contribution of the Compton effect could contribute to the HEW, *it should not be the main responsible for the divergence of the HEW after 27 keV* in the present PANTER dataset.

Tab. 4: evaluation of the impact of Compton scattering on the image degradation in the pn-EPIC detector. The Compton energy shift is included in the simulation. The photoelectric efficiency is in good agreement with the pn-EPIC tabulated values.

| Energy (keV)  | 5    | 10   | 15   | 20   | 25   | 30   | 35   | 40   | 45   | 50   |
|---|------|------|------|------|------|------|------|------|------|------|
| Photoelectric efficiency (%)                                | 99.9 | 89.3 | 48.8 | 24.4 | 13.1 | 7.7  | 4.8  | 3.2  | 2.2  | 1.59 |
| Compton efficiency (%)                                      | 1.42 | 1.40 | 1.39 | 1.38 | 1.38 | 1.37 | 1.37 | 1.38 | 1.39 | 1.36 |
| Fraction of detected photons after a Compton scattering (%) | 1.42 | 1.21 | 0.75 | 0.45 | 0.29 | 0.19 | 0.14 | 0.10 | 0.08 | 0.06 |
| Compton contribution to HEW (arcsec)                        | 0.0  | 0.0  | 0.1  | 0.3  | 0.5  | 1.0  | 1.5  | 2.2  | 2.9  | 3.5  |



|   |   |          |       |                     |          |
|---|---|----------|-------|---------------------|----------|
|   | <p align="center"><i>Multilayer Coatings for High-Energy Optics for Astrophysics</i></p> <p align="center"><b>Optics 346 manufactured at MSFC and Harvard-CfA: results of tests at PANTER facility and surface characterization</b></p> |          |       |                     |          |
| Code:01/07  | INAF/OAB Technical Report   | Issue: 1 | Class | <b>CONFIDENTIAL</b> | Page: 16 |

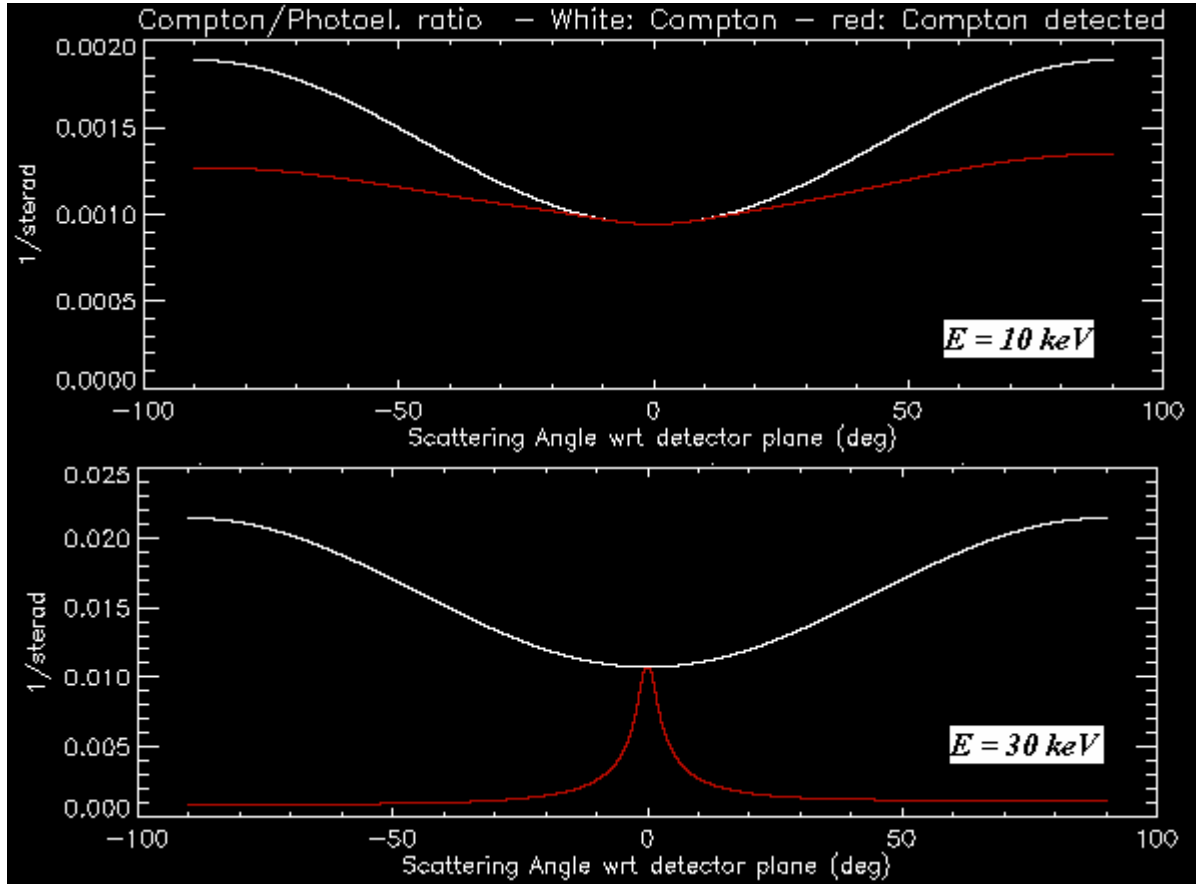



Fig. 10: comparison of the distribution of detected photons after a Compton scattering at 10 keV (top) and 30 keV (bottom), divided by the primary photoelectric efficiency of the detector. As  $E \ll 511$  keV, the Compton distribution (white) in normal incidence exhibits the typical dipolar pattern. At 10 keV, the Compton scattering efficiency is very low with respect to the primary photoelectric effect, even though most scattered photons are re-detected (red). At 30 keV the Compton scattering is 10 times more important: indeed, most scattered photons escape from the detector, except those lying in directions close to the detector plane.

### 3.2.2- X-ray scattering from surface microroughness

Another explanation for the trend of the HEW is the X-ray scattering from the surface microroughness. We consider the measured HEW as the sum of two terms: the HEW caused by the mirror figure errors (independent on the photon energy)  $HEW_{fig}$  and the energy-dependent term  $H(\lambda)$  due to the X-ray scattering. The two HEW are combined [RD5] to return the measured HEW:

$$HEW_{meas}^2 \approx HEW_{fig}^2 + H(\lambda)^2$$

if one assumes the X-ray scattering to be negligible at low energies, a  $HEW_{fig}$  value of 26 arcsec can be obtained from an extrapolation of the trend to  $E$  (see Fig.11). We have therefore to justify the trend  $H(\lambda)$  as a function of the energy. The values of  $H(\lambda)$  are reported in Tab. 5 and in Fig. 12 (left). Also

|  |   |          |       |                     |          |
|--|---|----------|-------|---------------------|----------|
|  | <p align="center"><i>Multilayer Coatings for High-Energy Optics for Astrophysics</i></p> <p align="center"><b>Optics 346 manufactured at MSFC and Harvard-CfA: results of tests at PANTER facility and surface characterization</b></p> |          |       |                     |          |
| Code:01/07   | INAF/OAB Technical Report   | Issue: 1 | Class | <b>CONFIDENTIAL</b> | Page: 17 |

the HEW term due to the Compton scattering term (see Tab. 4) could be also subtracted (however, the effects would be negligible).

We can infer from the measured PSD the values of the HEW scattering term, but in this case it is convenient to perform the inverse operation. For a double reflection optic, neglecting the finite source distance and the scattering modulation due to the presence of the multilayer, and provided that  $H(\lambda) \ll \theta_i$ , the PSD  $P(f)$  can be computed from the values of  $H(\lambda)$ , the PSD can be inferred from the differential equation [RD5] (*D. Spiga, A&A*):

$$\frac{P(f)}{\lambda} \frac{d}{d\lambda} \left( \frac{H(\lambda)}{\lambda} \right) = - \frac{\ln(4/3)}{4\pi^2 \sin^3 \vartheta_i}$$

and the spatial frequencies  $f$  are simply calculated from the formula

$$f = H(\lambda) \frac{\sin \vartheta_i}{2\lambda}$$

The PSD calculated from the  $H(\lambda)$  trend, that covers a spectral range from 15 mm to 60  $\mu\text{m}$ , is plotted in Fig. 12 (right), and the agreement with the topographical set of data is satisfactory. The remaining discrepancy can be ascribed to the some uncertainty in the WYKO PSD. We can therefore conclude that the measured HEW trend is caused by the mirror surface microroughness. Moreover, the divergence of HEW after 27 keV falls at the PSD “ankle” around 300  $\mu\text{m}$ : hence the steep degradation of the imaging quality is due to the very small spectral index at higher frequencies and the consequent roughening in the AFM spectral range.

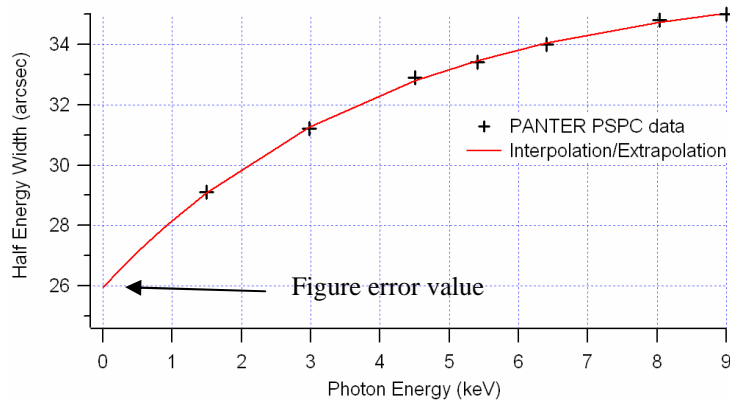




Fig. 11: Extrapolation of the low-energy HEW to  $E=0$  in order to recover the figure error contribution.

Tab. 5: measured HEW and the scattering contribution  $H(\lambda)$  derived from it with a subtraction in quadrature of 26 arcsec figure error

| keV  | 0.93 | 1.49 | 2.98 | 4.51 | 5.41 | 6.40 | 8.05 | 9.0  | 16.0 | 21.0 | 27.0 | 29.0 | 32.0 | 37 |
|--|------|------|------|------|------|------|------|------|------|------|------|------|------|----|
| HEW  | 28.8 | 29.1 | 31.2 | 32.9 | 33.4 | 34.0 | 34.8 | 35   | 38.0 | 39.0 | 42.0 | 51.0 | 61.3 | 85 |
| $(\text{HEW}^2 - \text{HEW}_{\text{fig}}^2)^{1/2}$ | 12.4 | 13.1 | 17.3 | 20.2 | 20.9 | 21.9 | 23.2 | 23.4 | 27.7 | 29.1 | 33.0 | 43.9 | 55.5 | 81 |

|   |   |          |       |                     |          |
|---|---|----------|-------|---------------------|----------|
|   | <p style="text-align: center;"><i>Multilayer Coatings for High-Energy Optics for Astrophysics</i></p> <p style="text-align: center;"><b>Optics 346 manufactured at MSFC and Harvard-CfA: results of tests at PANTER facility and surface characterization</b></p> |          |       |                     |          |
| Code:01/07  | INAF/OAB Technical Report   | Issue: 1 | Class | <b>CONFIDENTIAL</b> | Page: 18 |

The PSD at smaller wavelengths cannot be measured from HEW data with the actual setup (a measurement at higher energies would be required to do this, or the W90 should be measured instead of HEW): however, we can at least infer that *the roughness rms at wavelengths between 60  $\mu\text{m}$  and 8.5  $\mu\text{m}$  should be 5.3  $\text{\AA}$* . The limit of 8.5  $\mu\text{m}$  corresponds to the scattering at the boundary of the ROI (i.e., 250 arcsec radius) used to compute the HEW, computed at 37 keV by means of the grating formula. The numerical integration of the PSD obtained from AFM measurement shows that the roughness between 60.5  $\mu\text{m}$  and 8  $\mu\text{m}$  has the value of 6.1  $\text{\AA}$ . The larger value (by 0.8  $\text{\AA}$ ) is probably due to a local fluctuation of the roughness. Also the error in measuring the HEW at high energies can sensitively affect the calculation.

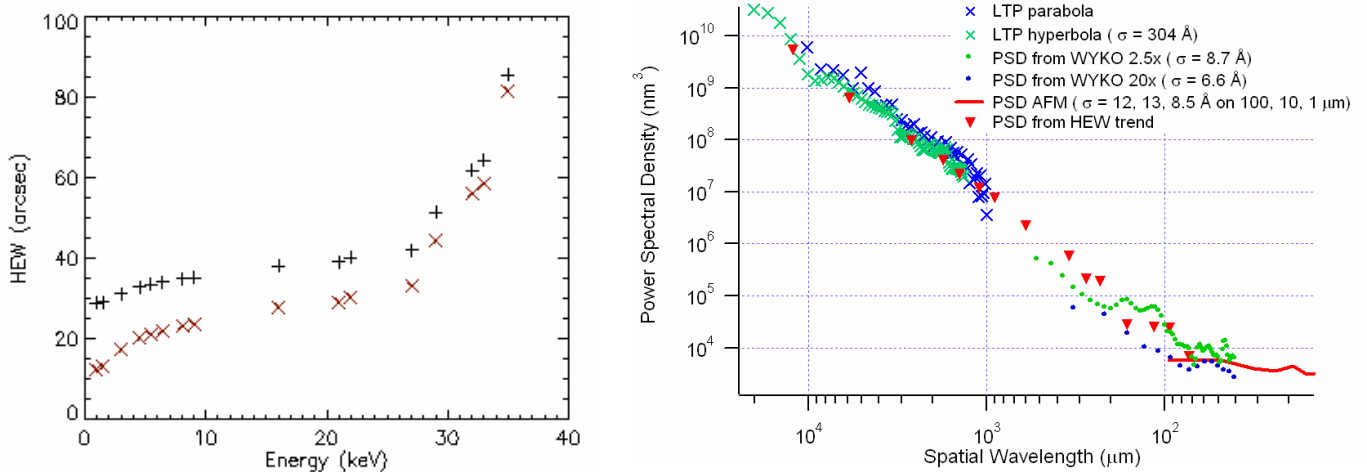


Fig. 12: (left) the measured HEW trend (black +) and the contribution of X-ray scattering (red x) assuming 26 arcsec of figure errors HEW. (right). The PSD of the mirror surface as reported in Fig. 9 (solid line). The PSD inferred from the scattering HEW term is also overplotted (marks). Notice the data matching.

### 3.3 – Conclusions

- ✓ The measured effective area values are consistent with the measured PSD over the investigated frequency range.
- ✓ The measured values of the HEW find an explanation in the X-ray scattering microroughness, provided that it is analyzed in terms of PSD over a wide interval of spatial frequencies. The PSD derived from the HEW trend is in good agreement with the measured one using the available topographical instrumentation.
- ✓ The low-frequencies PSD, with its high spectral index, causes a slow increase of HEW at photon energies smaller than 27 keV.
- ✓ The main responsible for the large HEW beyond 27 keV and for the effective area values being measured is the roughness at spatial periods smaller than 60  $\mu\text{m}$ , due to surface defects that are - probably - already present on the replicated mirror shell. The roughness in this spatial frequencies interval has to be smoothed in order to sensitively improve the optical performances.